

A Volume-Based Contact Dynamics Model with Asymmetric Damping Independent of the Coefficient of Restitution

André Roy¹, Juan A. Carretero²

¹Dept. of Mechanical Eng., U. of New Brunswick, Fredericton, NB, E3B 5A3, Email: Andre.Roy@unb.ca

²Dept. of Mechanical Eng., U. of New Brunswick, Fredericton, NB, E3B 5A3, Email: Juan.Carretero@unb.ca

Abstract

A novel contact dynamics model is presented that uses information about the interference geometry to predict contact forces. The interference volume is shown to be an analogue of the deformations of the Winkler elastic foundation model and is compared to the Hertz model for validity.

The inherent problems the Kelvin-Voigt model exhibits disappear when used to replace each spring in the Winkler elastic foundation. This introduces deformation rate effects into the Winkler elastic foundation model whose volumetric analogue is the rate of change of the volume of interference. When derived in this manner, the contact model becomes independent of the coefficient of restitution. The Hunt-Crossley model's damping term formulation is then discussed and compared to the model proposed here. Even though the model is general, the geometries used in the examples are cylindrical or spherical because they are easy to understand and easy to reproduce.

Keywords: simulation, contact dynamics, asymmetric damping, Hunt-Crossley, interference volume, volume-based model.

Un modèle pour la dynamique de contact basé sur le volume d'interférence avec amortissement asymétrique et indépendance du coefficient de restitution

Résumé

Un nouveau modèle de dynamique de contact est présentée qui utilise des informations sur l'interférence géométrique afin de prédire les forces de contact. Le volume d'interférence est présenté comme un analogue exact de la déformation de la fondation élastique du modèle Fondation Élastique de Winkler et le modèle est comparé au modèle de Hertz.

Les problèmes inhérents du modèle de Kelvin-Voigt disparaissent lorsqu'il est utilisé pour remplacer chaque ressort dans la fondation élastique de Winkler. Cela introduit des effets de vitesse de déformation sur le modèle élastique de Winkler dont le modèle analogue de à base de volume est le taux de variation du volume d'interférence. Lorsque il est dérivé de cette manière, le modèle de contact devient indépendant du coefficient de restitution. Le terme d'amortissement sur la formulation de Hunt-Crossley est ensuite discutées et comparé au modèle proposé dans cet article. Même si le modèle présenté est général, les géométries utilisées dans les exemples sont cylindriques ou sphériques, parce qu'elles sont faciles à comprendre et faciles à reproduire.

Mots-clé: simulation, dynamique de contact, amortissement asymétrique, Hunt-Crossley, modèle à base de volume, interférence géométrique.

1 INTRODUCTION

There are three important continuous contact models which are based on penetration distance or depth [1]; the Kelvin-Voigt model, the Hertz model, and the Hunt-Crossley model. The Kelvin-Voigt model states that the contact force is:

$$\begin{aligned} f_{\hat{n}} &= f_{\hat{n}_s} + f_{\hat{n}_d} \\ &= k\chi + b\dot{\chi} \end{aligned} \quad (1)$$

where $f_{\hat{n}_s}$ and $f_{\hat{n}_d}$ are the stiffness and damping portions of the normal contact force respectively, k is the material stiffness coefficient, b is the material damping coefficient, χ is the penetration depth and $\dot{\chi}$ is the penetration rate. There are three commonly stated problems with this model [1, 2, 3, 4]. They are (see Figure 1):

- the damping force is not zero upon initial contact (point f_1),
- the forces between the objects exhibit tension right before leaving contact (segment from f_2 to f_3), and,
- the coefficient of restitution is not dependent on the impact velocity as has been empirically determined.

The Hertz Model [1, 5] increased the accuracy of the stiffness portion of the contact force by approximating the stress distribution in the contact region based on the contact surface geometry and the penetration depth χ . The contact force, as approximated by [3] for identical spheres, is determined using:

$$f_{\hat{n}} = k\chi^n, \quad (2)$$

where, n , a geometry constant, was determined to be $\frac{3}{2}$ for the case of linearly elastic spheres [3, 6]. This Hertzian formulation for the stiffness portion of the contact force was introduced as the basis for the Hunt-Crossley model which can be written using the damping constant λ as:

$$f_{\hat{n}} = k\chi^n + \lambda\chi^p\dot{\chi}^q, \quad (3)$$

where q and p are generally set to 1 and n , respectively [1]. By making the damping portion (*i.e.*, the second term in equation (3)) dependent on the penetration depth, Hunt and Crossley were able to resolve the common contact problems experienced by the Kelvin-Voigt model such zero contact forces at the onset and offset of the contact (see Figure 2). It has been shown [1, 3] that for the central impact of two bodies at low impact velocities, the effective coefficient of restitution e_e , the ratio between the initial and final impact velocities, can be expressed as:

$$e_e = 1 - \alpha\dot{\chi}_i \quad (4)$$

where $\dot{\chi}_i$ is the penetration rate at initial impact and α is an empirically determined factor valid for a limited range of impact velocities. This leads to the following equation for λ :

$$\lambda = \frac{3}{2}\alpha k. \quad (5)$$

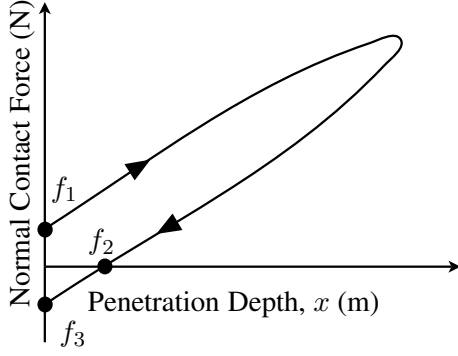


Figure 1: Contact-force cycle of the Kelvin-Voigt model.

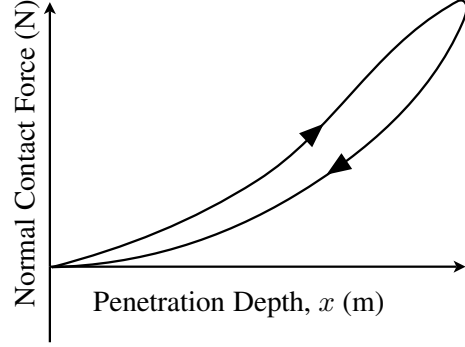


Figure 2: Contact-force cycle of the Hunt-Crossley model.

This result for λ has been corroborated using a few different methods [2, 4]. However, it was shown that λ is more accurately defined as:

$$\lambda = \frac{kd}{e_e \dot{\chi}_i} \quad (6)$$

where e_e is the effective coefficient of restitution and $d = \alpha e_e \dot{\chi}_i$ is a damping term [6]. A relationship between d and e_e independent of $\alpha \dot{\chi}_i$ was then derived. Examples of coefficients of restitution vs. impact velocity graphs can be found in [4, 7].

A link between the deformations of the Winkler elastic foundation model and the volume of interference has been made in [8] where the authors used the Hunt-Crossley model for the damping term resulting in:

$$f_{\hat{n}} = (k/h)V(1 + \alpha \dot{\chi}), \quad (7)$$

where h is the Winkler elastic foundation spring bed depth and V is the volume of interference between two interfering objects. This model includes both damping and elastic terms and will be referred to as the Gonthier *et al.*'s model.

Here, a damping term that is based on volumetric information and is also independent of the coefficient of restitution will be derived. This new contact dynamics model uses fundamental material deformation concepts in its formulation which provides a proper theoretical foundation. It will be shown that the damping term exhibits expected physical behaviour.

2 THE WINKLER ELASTIC FOUNDATION MODEL USING A KELVIN-VOIGT BED

The volume of interference between the contacting objects is an exact analogue of the inherent deformations in the bed of the Winkler elastic foundation model [8]. The deformation rate effects caused by damping can also be taken into account by extending the bed model to use both springs and dashpots. This creates an infinite amount of one-dimensional Kelvin-Voigt models spread in parallel under the contacting surfaces. Each differential volume in the volume of interference is then modelled as a spring and dashpot (Figure 3) that is compressed down to the contact surface.

When two objects come into contact, a normal pressure field is formed between them. This pressure field is caused by the deformation of the two contacting bodies. Integrating the normal pressure over the contact area will provide the total normal restitutive force as:

$$f_{\hat{n}_s} = \int \sigma da, \quad (8)$$

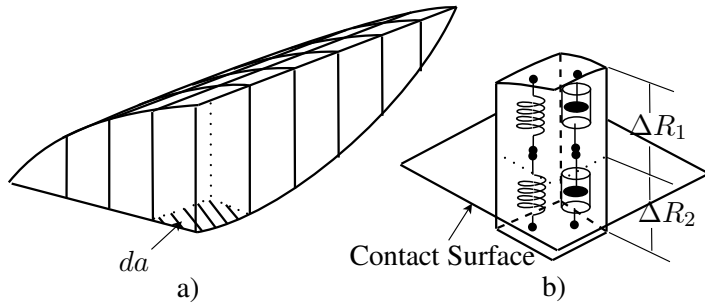


Figure 3: Volume of interference between two cylindrical objects: a) differential area associated with a differential volume, and b) a differential volume of interference showing its spring and damper representation.

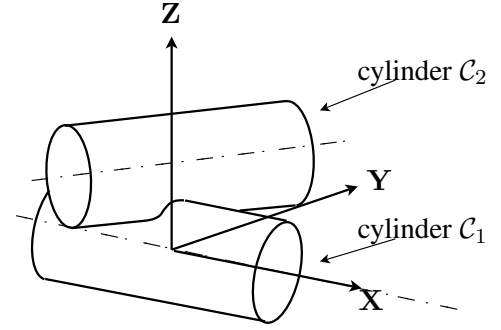


Figure 4: Frame definition for two intersecting cylinders.

where $f_{\hat{n}_s}$ represents the stiffness portion of the restitutional normal contact force, σ is the local pressure and da is the differential area the pressure is applied to.

The normal contact pressure is obtained from the material deformation which is approximated by the interference geometry's volume. For convenience, here are some intermediary derivations for the contact force between two cylindrical objects:

$$\sigma = Ee, \quad (9)$$

$$e = \frac{\Delta R}{R}, \quad (10)$$

$$dV = \Delta R da, \quad (11)$$

$$V = \int dV = \int \Delta R da, \quad (12)$$

where σ is the normal stress/pressure, E is the material's Young's modulus, e is the engineering strain, ΔR is the change in radius due to deformation at a point on the contact patch surface, R is the undeformed radius of the cylindrical object, da is the differential normal area and dV is the differential volume (see Figure 3). Although the model is certainly not limited to them, the geometries used in these examples will be cylindrical or spherical because they are easy to understand and easy to reproduce. The volume V , is the sum of all the penetration depths times their differential areas and it approximates the actual deformation of *both* cylindrical objects. That is, the surface of both cylindrical objects only deforms to meet partway at the contact surface. Therefore, the volume of interference V represents the deformation of cylinder C_1 due to the contact as well as the deformation of cylinder C_2 . If the material properties and radius of both cylinders were identical, the deformation in each cylinder would be identical as well. Therefore, only half of the total interference volume would need to be used to obtain the contact force applied to each cylinder. The normal force $f_{\hat{n}}$ on one cylinder could then be expressed as:

$$f_{\hat{n}_s} = \frac{EV}{2R}. \quad (13)$$

This formulation only holds true for small interference volumes because of the use of the engineering strain (equation (10)), which itself only holds true when $\Delta R \ll R$.

Using the same type of derivation, a damping effect can be added using the strain rate:

$$f_{\hat{n}_d} = B \int \dot{\epsilon}^m da, \quad (14)$$

where B is the damping factor (often referred to as the strain hardening coefficient), m is the strain rate sensitivity exponent [9]. The radial engineering strain rate for cylindrical objects, along the contact plane normal to the axes of both cylinders, is defined as:

$$\dot{\epsilon} = \frac{1}{R} \frac{d(\Delta R)}{dt}, \quad (15)$$

where $\frac{d(\Delta R)}{dt}$ is the radial deformation rate of the cylinder.

When dealing with cylinders of dissimilar materials, more specifically when the strain rate sensitivity of cylinder \mathcal{C}_1 (m_1) is different than that for cylinder \mathcal{C}_2 (m_2), it becomes difficult to obtain the damping component of the contact force independent of the velocity of the contact surface. On the other hand, when the damping component is linear (*i.e.*, $m_1 = m_2 = 1$) this is no longer an issue. Linear damping or simply identical strain rate sensitivity exponents for the material of the objects in contact must therefore be a fundamental assumption. Equation (13), for similar materials, linear damping and cylinder radii, then becomes:

$$f_{\hat{n}} = \frac{EV}{2R} + \frac{B}{2R} \frac{dV}{dt}, \quad (16)$$

where $\frac{dV}{dt}$ is the rate of change of the volume of interference with respect to time.

Equation (13) can be modified to account for dissimilar materials and radii resulting in:

$$f_{\hat{n}_s} = \frac{E_1 E_2 V}{R_2 E_1 + R_1 E_2}, \quad (17)$$

where E_i is the Young's Modulus of cylinder \mathcal{C}_i and R_i is the radius of cylinder \mathcal{C}_i . Again, considering the linear damping component, equation (16) becomes:

$$f_{\hat{n}} = \frac{V E_1 E_2}{R_2 E_1 + R_1 E_2} + \frac{dV}{dt} \frac{B_1 B_2}{R_2 B_1 + R_1 B_2}, \quad (18)$$

where B_i is the damping factor of the material of cylinder \mathcal{C}_i .

2.1 Elliptical Projection of the Geometry of Interference onto the Axial Plane

In order to determine the contact geometry, a Cartesian reference frame is first defined. As shown in Figure 4, the \mathbf{Z} axis is placed co-linear with the line segment defining the shortest distance between the axes of the two cylinders. The direction of \mathbf{Z} can be easily obtained as the cross-product of both cylinder's axes. Next, the \mathbf{X} axis is defined co-linear to the axis of cylinder \mathcal{C}_1 , while the origin of the frame is located at the point on cylinder \mathcal{C}_1 where the distance between it and cylinder \mathcal{C}_2 is shortest. Being a Cartesian coordinate system, the \mathbf{Y} axis can be found as $\mathbf{Y} = \mathbf{Z} \times \mathbf{X}$.

The projection of the interference geometry of two identical infinite cylinders onto the axial plane, whose axes are perpendicular to each other, takes a circular shape (see Figure 5). If one of those cylinder's radius is varied, then the projection takes on an elliptical shape with the major

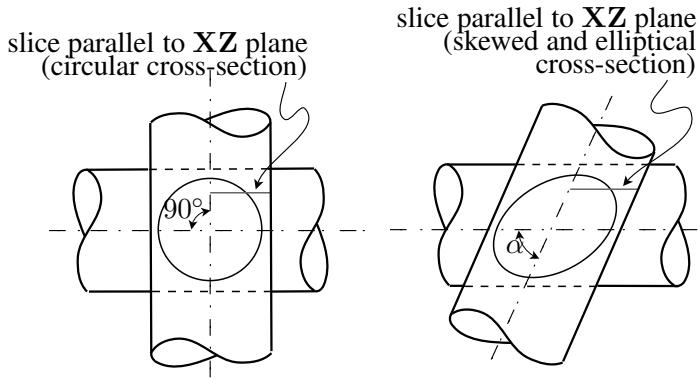


Figure 5: The skewing and scaling effect of the contact patch with the skewing of the axes of the contacting cylinders.

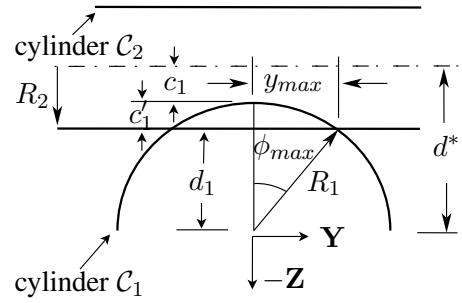


Figure 6: Two interfering cylinders, highlighting some important descriptive parameters.

axis aligned with the axis of the smaller cylinder. Also, when the angle between the cylinders is varied, the original circular projection becomes skewed and is stretched in the \mathbf{X} direction. This is because as cylinder \mathcal{C}_2 rotates, any slice parallel to the \mathbf{XZ} plane skews with the axis of cylinder \mathcal{C}_2 . Because a slice parallel to the \mathbf{XY} plane of the skewed cylinder \mathcal{C}_2 is elliptical, the interference geometry projection also stretches.

The dimensions of the original, non skewed or stretched, interference geometry projection are easily obtained. The radius of the interference volume in the \mathbf{Y} direction, y_{max} , is derived as follows:

$$\begin{aligned} d_1 &= d^* - R_2, \\ \phi_{max} &= \arccos(d_1/R_1), \\ y_{max} &= d_1 \tan(\phi_{max}) \end{aligned} \quad (19)$$

where all the dimensions are defined in Figure 6.

The radius of the original interference geometry projected in the \mathbf{X} direction, *i.e.*, x_{max} , is obtained in a similar fashion.

The shape of the projection of the interference geometry, being elliptical in nature, can be described as follows:

$$x(\theta) = x_{max} \cos(\theta) / \cos(\alpha) + y(\theta) / \tan(\alpha), \quad (20)$$

$$y(\theta) = y_{max} \sin(\theta), \quad (21)$$

where $x_{max} \cos(\theta)$ is the component in the \mathbf{X} direction of the undeformed elliptical projection. This projection is stretched by $1/\cos(\alpha)$ to take into account the elliptical nature of a slice parallel to the \mathbf{XZ} plane, and skewed by $y(\theta) / \tan(\alpha)$, where α is the smaller angle between the cylinder's axes as projected onto the \mathbf{XY} plane.

Using equations (20) and (21), an equation for the length of a vector $l(\theta)$, between the origin of the reference frame and $(x(\theta), y(\theta))$ can be found:

$$l(\theta) = \sqrt{x^2(\theta) + y^2(\theta)}. \quad (22)$$

Setting $\frac{dl(\theta)}{d\theta} = 0$ and solving for θ provides the location and size of the major and minor axes of the elliptical projection on the \mathbf{XY} plane of the interference geometry between two cylinders of arbitrary radius and orientation.

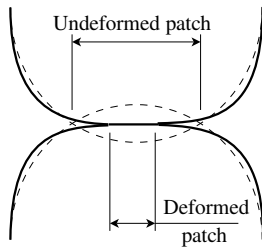


Figure 7: A qualitative comparison of two contacting cylinders undeformed (dashed lines) and deformed by contact pressure (solid lines).

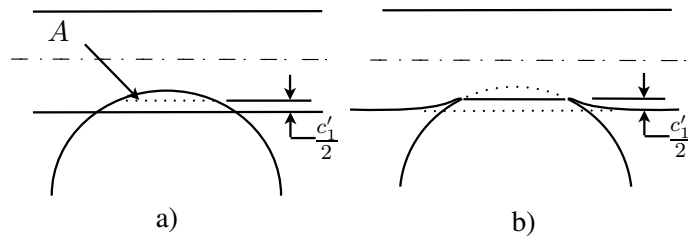


Figure 8: Two intersecting cylinders showing a) their undeformed state and the plane A where the surface would meet under deformation and b) the deformed cylinders after deformation.

2.2 A Comparison of Hertz to Winkler Elastic Foundation Model

In order to verify the accuracy of the force obtained through the volume of interference, it was compared with the Hertzian model of general contact³. The force provided through the volume of interference model is used in the Hertzian model to provide the major and minor axes of the elliptical contact patch. The contact patch area is then compared to the contact patch area from the volumetric model and a relationship between the two was determined.

In this section and in order to illustrate this concept, an example with two contacting straight cylinders is used. This example simplifies the volume formulation as well as provides quadratic surfaces which the Hertzian contact model is well suited for [5].

Here, the contact patch for the volume of interference model is approximated as the projection of the interference geometry on the axial plane. Figure 7 shows the differences between the actual contact patch and the intersection geometry. A better approximation of this contact patch area may be to determine it by calculating the area of a slice of the interference geometry at the plane A located directly in the middle (see Figure 8a). This is true only when the contacting cylinders have identical radii and material properties, which is the case for this validation. That is, since it is assumed that the cylinders are made of the same material and have the same radius, the surface of both cylinders will deform equally, and hence meet half way at region A shown in Figure 8b. A fast way of estimating the area of A is by separating the cylinders by $\frac{c'_1}{2}$ as shown in Figure 8b and finding the elliptical area of the projection of its interference geometry as described earlier in this section.

Figure 9 shows the percentage differences between the contact patch areas of both methods. The model described here adheres to the Hertzian contact model at almost any angle α between the cylinders to within 5% as long as the penetration depth is less than 25% of the cylinder's radius. Both the Hertzian contact model as well as the volume of interference model, assume small deformations.

³Hertzian contact theory can use the geometry of the contact patch as input in order to provide a force [5, 10].

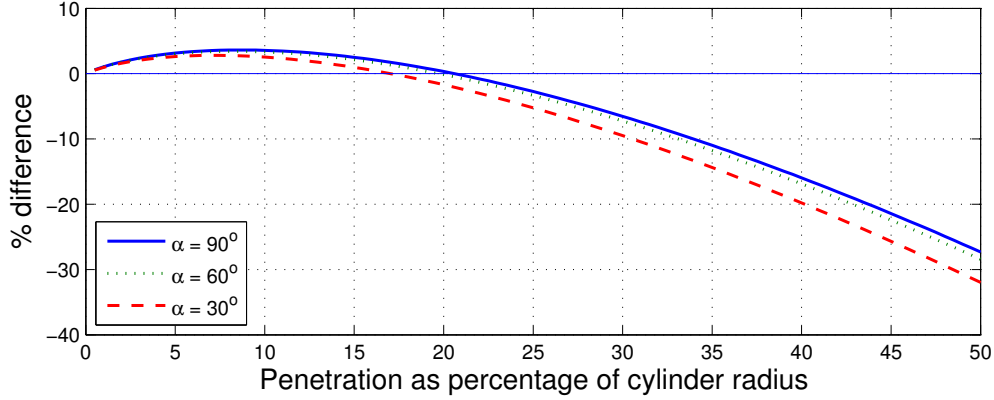


Figure 9: Percentage difference between contact patch area of the Hertzian model and the contact patch area from the interference geometry for three different angles between the cylinders.

3 DISCUSSION

It has been shown that the Winkler elastic foundation model adheres fairly well to the Hertz model. Hertz-based models, and therefore the Hunt-Crossley’s model, approximate the stress distribution based on the maximum penetration depth and based on the geometry of the contacting surfaces. In fact, this is also what the Winkler elastic foundation model does, so it’s not surprising that the results are similar.

The damping portion of the Winkler elastic foundation model also approximates the stress distribution based on the distribution of the rate of change of the strain. In order to compare the damping term in the Hunt-Crossley and Gonthier *et al.* to the one proposed here, the term $\frac{dV}{dt}$ in equation (16) is broken down into $\frac{dV}{d\chi} \frac{d\chi}{dt}$ or $\frac{dV}{d\chi} \dot{\chi}$ where χ refers to the penetration depth. Therefore, equation (16) can be expressed as:

$$f_{\hat{n}} = \frac{EV}{2R} + \frac{B}{2R} \frac{dV}{d\chi} \dot{\chi}. \quad (23)$$

For the case of two contacting spheres, $\frac{dV}{d\chi} = 0$ at $\chi = 0$. The Kelvin-Voigt model’s problem of a non-zero damping force upon initial impact is no longer an issue. With the Kelvin-Voigt model, when the damping term becomes larger than the stiffness term, an elastic force is exhibited. This elastic force is not physically possible as the contacting surfaces are not attached to each other. For example, taking two “fully-penetrated” objects at zero velocity, the two objects will start to accelerate away from each other, the stiffness component will reduce to zero as the penetration depth decreases to zero, while the damping force will increase from zero as the velocity increases. When the damping term completely cancels out the stiffness term, the contact surfaces can no longer accelerate outwards and therefore can no longer impart forces onto the opposite object. From this point on, the object will continue on their travel at a constant velocity while the contact surfaces decelerate and are eventually restored to their original positions [11].

Finally, the coefficient of restitution must be dependent on velocity. The coefficient of restitution versus the impact velocity behaviour of this model (see Figure 10) shows similar results to those in [4] and [7]. For low impact velocities, the coefficient of restitution is linearly dependent on

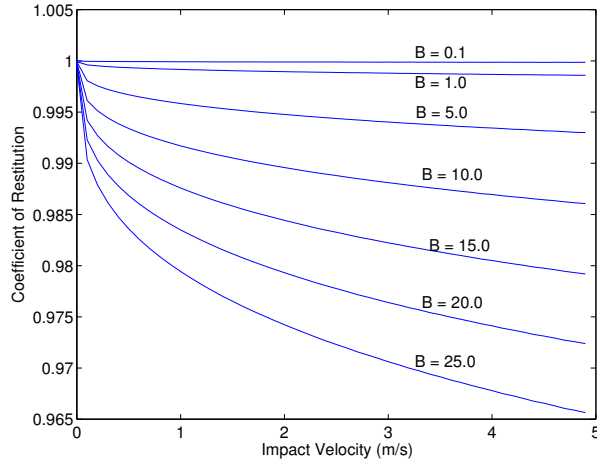


Figure 10: The coefficient of restitution vs. impact velocity for two impacting spheres: radius $R = 1\text{ m}$, mass $m = 0.454\text{ kg}$, spring constant $E = 200,000 \frac{\text{N}}{\text{m}^2}$ with varied damping constants B in $\frac{\text{Ns}}{\text{m}^2}$ (Kelvin-Voigt Winkler Elastic Foundation Model).

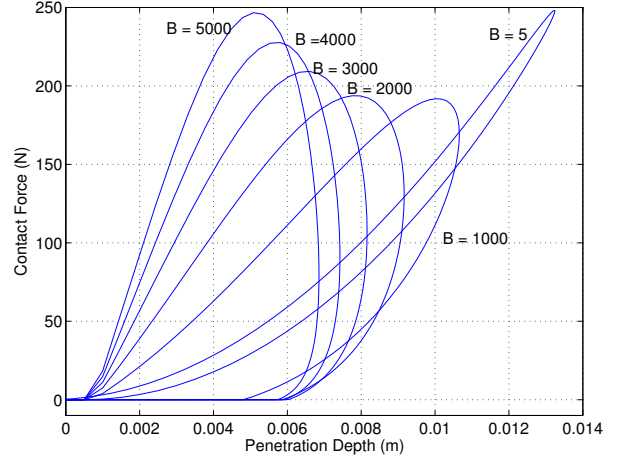


Figure 11: The contact force vs. penetration depth of two impacting spheres: radius $R = 1\text{ m}$, mass $m = 0.454\text{ kg}$, spring constant $E = 200,000 \frac{\text{N}}{\text{m}^2}$, velocity $\dot{\chi} = 1 \frac{\text{m}}{\text{s}}$ with varied damping constants B in $\frac{\text{Ns}}{\text{m}^2}$ (Kelvin-Voigt Winkler Elastic Foundation Model).

impact velocity as empirically determined because the deformation rate $\frac{dV}{d\chi}$ is practically linear for small χ [3].

Figure 11 shows the effect of the damping factor on the contact force. When the ratio E/B becomes smaller, the energy loss, *i.e.*, the area inside the contact loop, is greater. The penetration depth at which the two spheres leave contact is obvious. Figure 12 shows a continuous power transfer like that exhibited by Hunt-Crossley's model and Gonthier *et al.*'s model, where power transfer refers to the rate of work done of one object done on the other taking into account the relative direction of travel from one another.

Comparing equations (7) and (23), one big difference that stands out is that equation (7) has the volume V in the damping term while equation (23) has a $\frac{dV}{d\chi}$ term instead. When $\chi \approx 0$, $\frac{dV}{d\chi} \approx V$ which means that both equations are equivalent, however, as the penetration depth increases, the less accurate the $\frac{dV}{d\chi} \approx V$ approximation becomes.

As demonstrated in [8], $V \approx \chi^{\frac{3}{2}}$ for two contacting spheres with small values of χ . As a result, $\frac{dV}{d\chi} \approx \frac{3}{2}\chi^{\frac{1}{2}}$ which coheres with the findings in [12] and [13]. Modifying the Hunt-Crossley model in this way would provide results closer to the ones proposed here. However, some of the derivations used to demonstrate the Hunt-Crossley model's appropriateness would become much harder. The damping term proposed here, overcomes the requirement of small penetration distances for accurate damping due to the assumption that $\frac{dV}{d\chi} \approx V$ when $\chi \approx 0$.

4 CONCLUSION

A new contact dynamics model that exhibits non-linear, asymmetric damping that is independent of the coefficient of restitution is proposed. The validity of the use of the volume of interference as an approximation of the stress distribution was shown through a comparison with Hertz theory

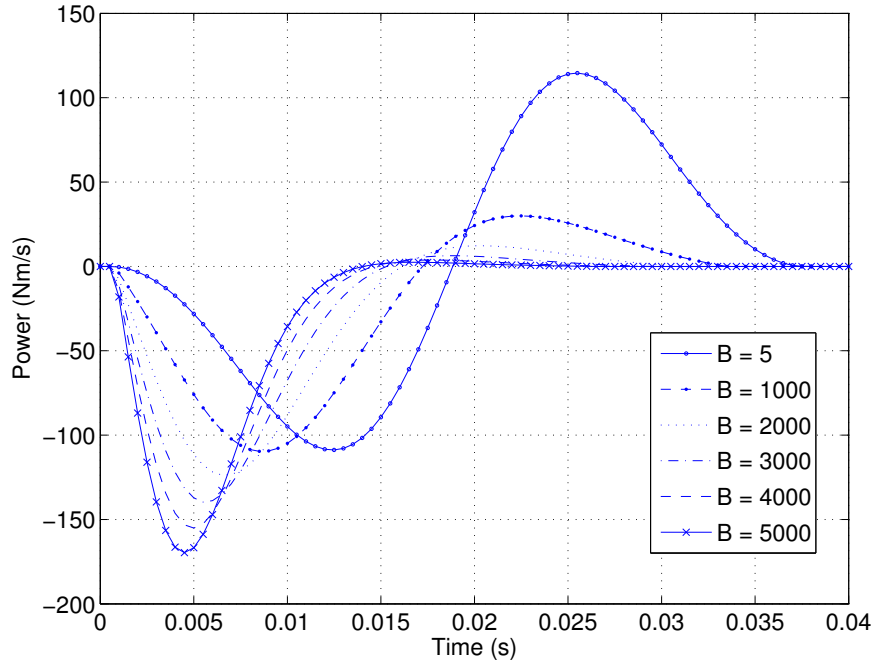


Figure 12: The power exchange vs. time of two impacting spheres: radius $R = 1m$, mass $m = 0.454kg$, spring constant $E = 200,000\frac{N}{m^2}$, velocity $\dot{\chi} = 1\frac{m}{s}$ with varied damping constants B in $\frac{Ns}{m^2}$ (Kelvin-Voigt Winkler Elastic Foundation Model).

of general contact.

The model builds on the findings of Gonthier *et al.* [8]. An analysis of the assumptions made for the Hunt-Crossley based damping model of [8] was undertaken and an alternate damping model is proposed which overcomes some of the inherent requirements of small penetrations for accuracy.

It was shown that, when a number of Kelvin-Voigt spring-damper models are used in parallel in a Winkler elastic foundation, the adverse effects exhibited with a single spring-damper are resolved. The proposed model behaves similarly to the Hunt-Crossley model yet more accurately since it removes the assumption that the contact forces are exhibited as long as the undeformed objects are interpenetrating. This is not the case because, as the objects accelerate away from each other, the damping portion of the contact force will eventually overpower the elastic force. When this happens, the contacting surfaces cease to impart forces onto one another [11]. It was also shown that the original Hunt-Crossley assumption to make $p = n$ (see equation (3)) may have been physically incorrect unless the $\chi \approx 0$ (at least for spheres) [12, 13].

The proposed model, based largely on the Winkler elastic foundation model with Kelvin-Voigt models used instead of its usual springs, exhibits a coefficient of restitution dependent on the impact velocity, and demonstrates asymmetric hysteretic damping. Yet, the damping coefficient is independent of the coefficient of restitution, rather it is an inherent, measurable material property. Though only cylindrical and spherical objects have been used in the numerical examples for simplicity, this method is applicable generally as long as the Winkler elastic bed depth can be defined.

REFERENCES

- [1] G. Gilardi and I. Sharf. Literature survey of contact dynamics modelling. *Mechanism and Machine Theory*, 37(10):1213–1239, October 2002.
- [2] N. Diolaiti, C. Melchiorri, and S. Stramigioli. Contact impedance estimation for robotic systems. *IEEE Transactions on Robotics*, 21(5):925–935, Oct. 2005.
- [3] K. H. Hunt and F. R. E. Crossley. coefficient of restitution interpreted as damping in vibroimpact. *Journal of Applied Mechanics*, 42:440–445, June 1975.
- [4] D. W. Marhefka and D. E. Orin. A compliant contact model with nonlinear damping for simulation of robotic systems. *IEEE Transactions on Systems, Man, and Cybernetics – PART A: Systems and Humans*, 29(6):566–572, Nov 1999.
- [5] K. L. Johnson. *Contact Mechanics*. Cambridge University Press, 1987.
- [6] Y. Gonthier, J. McPhee, C. Lange, and J.-C. Piedboeuf. A regularized contact model with asymmetric damping and dwell-time dependent friction. *Multibody System Dynamics*, 11:209–233, 2004.
- [7] W. Goldsmith. *Impact: The Theory and Physical Behaviour of Colliding Solids*. Dover Publications, (1960) 2001.
- [8] Y. Gonthier, J. Mcphee, C. Lange, and J-C Piedboeuf. A contact modeling method based on volumetric properties. *Proceedings of IDETC'05 2005 ASME Design Engineering Technical Conferences and 5th International Conference on Multibody Systems, Nonlinear Dynamics and Control*, September 24-28 2005.
- [9] S. Kalpakjian and S. R. Schmid. *Manufacturing Processes for Engineering Materials*. Prentice Hall, 2003.
- [10] R. L. Norton. *Machine Design, An Integrated Approach*. Prentice Hall, 2000.
- [11] R. Cross. The bounce of a ball. *American Journal of Physics*, 67(3):222–227, March 1999.
- [12] E. Falcon, C. Laroche, S. Fauve, and C. Coste. Behavior of one inelastic ball bouncing repeatedly off the ground. *The European Physical Journal B*, 3:45–57, 1998.
- [13] G. Kuwabara and K. Kono. Restitution coefficient in a collision between two spheres. *Japanese Journal of Applied Physics*, 26(8):1230–1233, August 1987.